Mathematical and Computer Modelling 58 (2013) 344–354

Contents lists available at SciVerse ScienceDirect

Mathematical and Computer Modelling

journal homepage: www.elsevier.com/locate/mcm

Geometric programming approach to doping profile design optimization of metal-oxide-semiconductor devices

Yiming Li *, Ying-Chieh Chen

Parallel and Scientific Computing Laboratory, Department of Electrical and Computer Engineering, National Chiao Tung University, 1001 Ta-Hsueh Road, Hsinchu 300, Taiwan

ARTICLE INFO

Keywords:
Doping profile
Design optimization
Geometric programming
MOS devices

ABSTRACT

We study one-dimensional doping profile design optimization problem of metal-oxide-semiconductor (MOS) devices using a geometric programming (GP) technique. To model the explored optimal doping profile into a GP problem, the subthreshold swing is formulated as an objective function and the on- and off-state currents are considered as constraints for solving the corresponding optimal doping profile. The GP problem is a special type of convex optimization and is solved globally and efficiently using the existing numerical solvers in GGPLAB. The accuracy of optimized results is validated by comparing with numerical semiconductor device simulation. This approach provides a way to optimize doping problem which may benefit manufacturing of MOS devices.
© 2012 Elsevier Ltd. All rights reserved.

1. Introduction

Channel doping profile continuously plays an important role in determining current–voltage (I–V) characteristics of metal-oxide-semiconductor field-effect transistors (MOSFETs). In order to estimate a MOSFET's DC characteristic, a set of classical drift-diffusion (DD) equations has to be solved [1,2]; one-dimensional (1D) DD equations consist of:

$$\begin{cases} \dfrac{d^2\varphi}{dx^2} = -\dfrac{q}{\varepsilon_{si}}\,(p - n + N_D - N_A) \\ \dfrac{d}{dx}\left(-\mu_n n\dfrac{d\varphi}{dx} + D_n\dfrac{dn}{dx}\right) = R(n,p) \\ \dfrac{d}{dx}\left(\mu_p p\dfrac{d\varphi}{dx} + D_p\dfrac{dp}{dx}\right) = R(n,p), \end{cases} \tag{1}$$

where the first equation above is the Poisson equation, φ is the electrostatic potential, n and p are carrier concentrations, q is the elementary charge, ε_{si} is silicon permittivity, and N_D and N_A are ionized doping profiles. The second and third equations above are the electron–hole current continuity equations, where μ_n, μ_p, D_n, and D_p are electron–hole mobility and diffusion coefficient, and $R(n, p)$ is the carrier's generation and recombination [1,2]. The doping profiles, N_D and N_A, in the Poisson equation should be determined, so that the calculate device's characteristics can meet a given specification. The procedure to search proper doping profile is a time-consuming and complicated task generally.

Recent approaches were proposed to inversely recover a channel doping profile of MOS devices, such as current–voltage (I–V) and capacitance–voltage (C–V) methods [3,4] from device characterization methodology, optimization using such as simulation-based evolutionary techniques [5,6], and full numerical methods [7–11]. However, to obtain an acceptable

* Correspondence to: National Chiao Tung University, 1001 Ta-Hsueh Road, Hsinchu 300, Taiwan.
E-mail address: ymli@faculty.nctu.edu.tw (Y. Li).

0895-7177/$ – see front matter © 2012 Elsevier Ltd. All rights reserved.
doi:10.1016/j.mcm.2012.11.002

solution with best accuracy, simulation-based evolutionary technique requires the solution of device transport equations iteratively which costs a huge amount of CPU time. In the meanwhile, nonlinear numerical optimization approaches and engineering characterization may result in a case sensitive or local solution. Mathematically, if the inverse doping profile problem could be modeled as an optimization problem and solved for global solution, it may benefit the design and manufacturing of MOSFET devices.

A geometric programming (GP) is a type of mathematical optimization problem which is characterized by objective and constraint functions with a certain special mathematical form [12,13]:

$$\begin{aligned} &\min_x f_0(x) = \sum_{t=1}^{u_0} c_{0t} \prod_{j=1}^{n} x_j^{a_{0tj}} \\ &\text{s.t.}\, f_i(x) = \sum_{t=1}^{u_i} c_{it} \prod_{j=1}^{n} x_j^{a_{itj}} \le 1, \quad i = 1, 2, \ldots, m \\ &g_i(x) = \prod_{j=1}^{n} x_j^{b_{ij}} = 1, \quad i = 1, 2, \ldots, q \\ &x_j \ge 0, \quad j = 1, 2, \ldots, n, \end{aligned} \tag{2}$$

where the *posynomial* $f_0(x)$ containing u_0 terms is the objective function, and the *posynomials* $f_i(x)$ for $i = 1, 2, \ldots, m$ containing u_i terms represent m inequality constraints [12]. According to the definition of *posynomial*, all coefficients c_{it} for $i = 0, 1, \ldots, m$ and $t = 1, 2, \ldots, u_m$ are positive, and a_{itj} for $i = 0, 1, \ldots, m$, $t = 1, 2, \ldots, u_m$ and $j = 1, \ldots, n$ are real numbers. Problems with a GP form could be solved using an interior-point based algorithm in a computationally cost-effective manner [14]. GP was applied in designs of BJT devices and electronic circuits [15–19], except its diverse applications in management and engineering (see, for instance, [12,13] and references therein).

This work, for the first time, models the inverse channel doping problem as a GP form. For a given device specification of N-type MOSFET, the 1D channel doping profile from the interface of silicon and silicon dioxide to the maximum depletion width is inversely recovered by minimizing a special physical quantity, the subthreshold swing (SS) [1,2], of MOSFETs subject to given constraints of DC characteristics:

$$\begin{aligned} &\min SS \\ &\text{s.t.}\, N_{\min} \le N_A(x) \le N_{\max}, \quad 0 \le x \le W_{dm} \\ &I_{on} \ge I_{on\text{-}set} \\ &I_{off} \le I_{off\text{-}set}, \end{aligned} \tag{3}$$

where the $N_A(x)$ is a P-type doping profile, which is a positive function of distance x ranging from the interface ($x = 0$) to the maximum depletion width ($x = W_{dm}$), and subject to the background doping level $N_{\min}$ which is limited by the maximum of doping concentration $N_{\max}$, as shown in Fig. 1. For the constraints in the problem (3), I_{on} denotes the on-state current, I_{off} is the off-state current, and $I_{on\text{-}set}$, $I_{off\text{-}set}$ are positive targeted specifications of I_{on} and I_{off}, respectively. For extracting the corresponding doping profile, as shown in Fig. 1(c), we first integrate the Poisson equation and derive the maximum depletion width which is a function of doping profile and is strongly affecting device DC characteristics [1,2]; the objective function SS is thus modeled accordingly. Furthermore, the on- and off-state currents are reformulated as *posynomial* inequalities in GP compatible constraints, then the studied inverse channel doping profile problem is well transformed to the GP one. The formulated GP problem is coded and solved together with the numerical solver in GGPLAB [14]. We optimize the channel doping profiles for different specifications of 0.35-μm MOSFET devices and obtain physically reasonable results. Note that for examining the result's accuracy of the developed optimization technique, the optimized doping profiles are further compared with device simulation [20,21] and the sensitivity of source and drain doping distributions are also estimated.

This paper is organized as follows. In the Section 2, starting from basic MOS device physics, we formulate W_{dm} and SS, the saturation and subthreshold currents as a GP program. In the Section 3, we perform numerical experiments and discuss the optimized results. Finally, we draw the conclusions and suggest future work.

2. The doping profile design optimization

In this section, the DC characteristics of MOSFETs are transformed to the *posynomial* functions, and thus the inverse doping profile problem (3) is formulated as a GP problem.

2.1. The integration of Poisson's equation

Generally, in the space charge region, the density of free electron $n(x)$ and hole $p(x)$ are almost zero, and the doping concentration of donor impurity $N_D(x)$ could be neglected in the Poisson equation of Eq. (1). Considering an integration

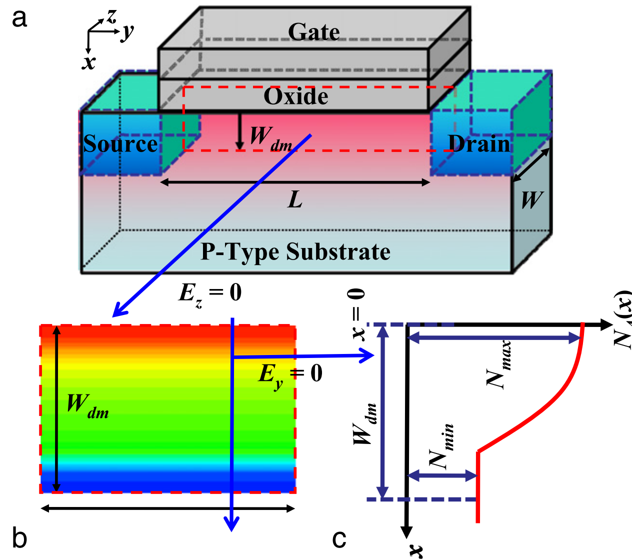

Fig. 1. (a) Illustration of MOSFET. (b) A slicing cut of the doping profile along the channel direction. (c) We solve the optimal doping profile from the interface of silicon and silicon di-oxide ($x = 0$) to the maximum depletion width ($x = W_{dm}$). The y-axis denotes the direction along the device channel length (L), the z-axis is along the device width (W) and the x-axis is along the device channel depth.

from x to the depletion width W_{dm}, we do neglect the y- and z-directions since the channel length L in the y-direction and device width W in the z-direction are assumed to be comparable large and, therefore, the electric field E_y and E_z are zero [1,2,22] as showed in Fig. 1(b). Under the approximations above, the 1D Poisson equation can be integrated as [1,2]:

$$2\psi_B = \frac{q}{\varepsilon_{si}} \int_0^{W_{dm}} x N_A(x) dx, \tag{4}$$

where ψ_B is the potential difference between Fermi level and intrinsic level [1]. One way to obtain the maximum depletion width is to discretize Eq. (4) for the maximum depletion width with K uniformly spaced points, as shown in Fig. 2, $x_j = jW_{dm}/K, j = 0, 1, \ldots, K$. The doping profile is then sampled at these points; we denote $d_j = N_A(x_j), j = 0, 1, \ldots, K$. Then, the approximated Eq. (4) is:

$$2\psi_B = \frac{q}{\varepsilon_{si}} \sum_{j=0}^{k} \left(\frac{jW_{dm}}{k}\right) d_j \left(\frac{W_{dm}}{K}\right) = \frac{q}{\varepsilon_{si}} \left(\frac{W_{dm}}{K}\right)^2 \sum_{j=0}^{K} j d_j, \tag{5}$$

therefore, the maximum depletion width W_{dm} can be further expressed as:

$$W_{dm} = K \sqrt{\frac{\varepsilon_{si} 2\psi_B}{q \sum_{j=0}^{K} i d_j}}, \tag{6}$$

which is a function of the discrete doping profile d_j owing to the potential difference between Fermi level and intrinsic level ψ_B, the silicon permittivity ε_{si}, and the elementary charge q are known physical constants.

2.2. The integration of carrier's current continuity equations

In Eq. (1), we integrate the total drain current density $J_{ds}(x, y)$ at steady state including both drift and diffusion components, and they are simplified as:

$$J_{ds}(x, y) = D_n n(x, y) \frac{dE_{Fn}}{dy}, \tag{7}$$

where the E_{Fn} is the minority-carrier quasi-Fermi potential [1]. Based on the total drain current density in Eq. (7) and the gradual-channel approximation, the total drain current I_{ds} is given by:

$$I_{ds} = W \int_0^{x} J_{ds}(x, y) dx = \frac{WD_n}{L} \int_0^{L} \frac{dE_{Fn}}{dy} \int_0^{x} n(x, y) dx dy. \tag{8}$$

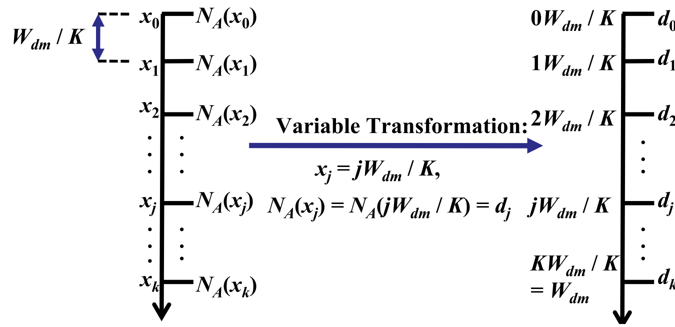

Fig. 2. The discretization and variables transformation of the integral (4).

In both the saturation and subthreshold regions [1], the integration of (8) can be derived as the saturation current I_{sat} and the subthreshold current I_{sub}, respectively:

$$I_{sat} = \frac{W}{2mL}\mu_n C_{ox}\left(V_{gs} - V_{fb} - 2\psi_B + \frac{Q_d}{C_{ox}} - \frac{V_{ds}}{2}\right)V_{ds}, \tag{9}$$

and

$$I_{sub} = \mu_{eff} C_{ox}\frac{W}{L}(m-1)\left(\frac{kT}{q}\right)^2 \exp\left(\frac{-q\left(V_{gs} + V_{fb} + 2\psi_B - \frac{Q_d}{C_{ox}}\right)}{mkT}\left(1 - e^{\left(\frac{-qV_{ds}}{kT}\right)}\right)\right), \tag{10}$$

where C_{ox} is the oxide capacitance per unit area, V_{gs} is the applied gate voltage, V_{ds} is the drain voltage, V_{fb} is the flat-band voltage, Q_d is the depletion charge, μ_{eff} is effective electron mobility, and m is the body-effect coefficient. The term $(V_{fb} + 2\psi_B - Q_d/C_{ox})$ appearing in Eqs. (9) and (10), is known as the threshold voltage V_t of the MOSFET device [1,2].

2.3. The objective function of subthreshold swing

The subthreshold swing (SS) is calculated by the subthreshold current of Eq. (10) which is changed by the gate voltage variation of one-order magnitude:

$$SS \equiv \left[\frac{d(\log_{10} I_{sub})}{dV_{gs}}\right]^{-1} = 2.3\frac{mkT}{q} = 2.3\frac{kT}{q}\left(1 + \frac{3t_{ox}}{W_{dm}}\right), \tag{11}$$

where t_{ox} is the oxide thickness. Substituting the maximum depletion width W_{dm} of Eq. (6) into Eq. (11), we can rewrite the expression of SS as:

$$SS = 2.3\frac{kT}{q}\left(1 + \frac{3t_{ox}}{K}\sqrt{\frac{q\sum_{j=0}^{K} jd_j}{2\varepsilon_{si}\psi_B}}\right). \tag{12}$$

The SS above satisfies the form of *posynomial* since the coefficients of all optimal variables d_j are positive. The transformation of SS is successfully performed into the form of *posynomial* and the requirement of SS is as small as possible in the device design; consequently, the SS is thus selected as the objective function in our GP problem (3).

2.4. The constraint of on-state current

To derive the constraint of on-state current [1,2] in the problem (3), we assume the saturation current of Eq. (9) to be larger than the specification of on-state current when $V_{dd} = V_{ds}$ (in this work, the on-state current is the target of saturation current when the applied drain voltage V_{ds} is equal to the power supply V_{dd}) and $V_{ds} = V_{gs} - V_t$:

$$\begin{aligned} I_{on} &= \frac{W}{2mL}\mu_{eff} C_{ox}(V_{gs} - V_t)^2 \\ &= \frac{W}{2mL}\mu_{eff} C_{ox}\left(V_{gs} - V_{fb} - 2\psi_B + \frac{Q_d}{C_{ox}}\right) \\ &\geq I_{on\text{-}set}, \end{aligned} \tag{13}$$

where the depletion charge Q_d is obtained from:

$$Q_d = -q \int_0^{W_{dm}} N_A(x) dx. \tag{14}$$

Using a similar procedure of discretization, as listed in Eqs. (4), (5) and (14) is approximated by the sum:

$$Q_d = -q \frac{W_{dm}}{K} \sum_{j=0}^{K} d_j. \tag{15}$$

According to the approximation above, we substitute Eq. (6) into Eq. (15), and Eq. (15) into Eq. (13), then Eq. (13) becomes:

$$\frac{\sqrt{2q\psi_B \varepsilon_{si}} \sum_{i=0}^{K} d_i}{C_{ox}\left(V_{gs} - \sqrt{\frac{2mI_{on\text{-}set}}{\left(\frac{W}{L}\right)\mu_{eff} C_{ox}}} - V_{fb} - 2\psi_B\right)} \le \sqrt{\sum_{i=0}^{K} jd_j}. \tag{16}$$

The denominator term on the left hand side of Eq. (16) ($V_{gs} - \sqrt{\frac{2mI_{on\text{-}set}}{(\frac{W}{L})\mu_{eff} C_{ox}}} - V_{fb} - 2\psi_B$) is positive owing to positive current of N-type MOS devices; however, this inequality in the present form is not a GP compatible constraint because the right-hand side of a *posynomial* inequality is not a constant or *monomial*. It is a direct result from the body-effect coefficient m depending on doping profile. We consider GP compatible constraints that approximately limit the doping profile for the constraint of on-state current. For the body-effect coefficient m, we use the maximum of doping concentration $N_{\max}$ to replace the doping concentration d_j in the expression of m and we have $m_{\max}$:

$$m_{\max} = 1 + \frac{3t_{ox}}{K} \sqrt{\frac{qN_{\max}\left(\frac{(K+1)(K+2)}{2}\right)}{2\varepsilon_{si}\psi_B}}. \tag{17}$$

Using $m_{\max}$ of Eq. (17) in Eq. (16), instead of m, we can guarantee the minimum of I_{on} (according to Eq. (13), as m goes large, the I_{ds} will become small) is greater than $I_{on\text{-}set}$, and the left-hand side of Eq. (16) will become a positive constant multiples a *posynomial* $\sum_{j=0}^{K} d_j$. For the term $\sum_{j=0}^{K} jd_j$ on the right-hand side, we use the arithmetic–geometric mean inequality to produce a GP compatible approximation for. Since the arithmetic mean is greater than geometric mean, we have:

$$\left(\prod_{j=0}^{K} id_j\right)^{\frac{1}{(K+1)}} \le \frac{1}{K+1} \sum_{j=0}^{K} jd_j; \tag{18}$$

therefore, if the inequality

$$\frac{\sqrt{2q\psi_B \varepsilon_{si}} \sum_{j=0}^{K} d_j}{C_{ox}\left(V_{gs} - \sqrt{\frac{2m_{\max}I_{on\text{-}set}}{\left(\frac{W}{L}\right)\mu_{eff} C_{ox}}} - V_{fb} - 2\psi_B\right)} \le \sqrt{(K+1)\left(\prod_{j=0}^{K} jd_j\right)^{\frac{1}{(K+1)}}} \tag{19}$$

holds, then the inequality (16) must also be satisfied. The inequality (19) is a GP compatible constraint, since the right-hand side is a *monomial* function with optimal variables d_j.

2.5. The constraint of off-state current

The off-state current I_{off} is a special case of the subthreshold current I_{sub} when V_{gs} = 0 and $V_{ds} = V_{dd}$ for example [1,2]. We assume the off-state current $I_{off} \le I_{off\text{-}set}$:

$$I_{off} = \mu_{eff} C_{ox} \frac{W}{L}(m-1)\left(\frac{kT}{q}\right)^2 \exp\left(\frac{q\left(-V_{fb} - 2\psi_B + \frac{Q_d}{C_{ox}}\right)}{mkT}\right) \le I_{off\text{-}set}. \tag{20}$$

Leaving the exponential term in the left-hand side, we replace m with $m_{\max}$ similarly to obtain the maximum I_{off} (according to Eq. (20), when m increases, I_{off} increases); and thus, we can guarantee $I_{off} \ge I_{off\text{-}set}$. Therefore, Eq. (20) is expressed as:

$$\exp\left(\frac{q\left(-V_{fb} - 2\psi_B + \frac{Q_d}{C_{ox}}\right)}{m_{\max}kT}\right) \le \frac{I_{off\text{-}set}}{\mu_{eff} C_{ox} \frac{W}{L}(m_{\max}-1)\left(\frac{kT}{q}\right)^2}. \tag{21}$$

The inequality (21) is not a GP compatible constraint because the *posynomial* function Q_d is in the exponential term. Therefore, we take logarithm to both sides of (21) and rearrange it as:

$$Q_d \geq C_{ox}\left(\frac{kTm_{\max}}{q}\ln\left(\frac{\mu_{eff}C_{ox}\frac{W}{L}(m_{\max}-1)\left(\frac{kT}{q}\right)^2}{I_{off\text{-}set}}\right)-V_{fb}-2\psi_B\right). \tag{22}$$

Following similar procedure in the last sub-section, we substitute Eq. (6) into Eq. (15), and Eq. (15) into Eq. (22), then Eq. (22) becomes:

$$\frac{C_{ox}}{q}\sqrt{\frac{\sum_{j=0}^{K} jd_j}{2q\psi_B\varepsilon_{si}}}\left(\frac{kTm_{\max}}{q}\ln\left(\frac{\mu_{eff}C_{ox}\frac{W}{L}(m_{\max}-1)\left(\frac{kT}{q}\right)^2}{I_{off\text{-}set}}\right)-V_{fb}-2\psi_B\right)\leq\sum_{j=0}^{K}d_j. \tag{23}$$

To obtain a valid *posynomial* inequality, we use the arithmetic–geometric mean inequality to transform the summation $\sum_{j=0}^{K} d_j$ in the right-hand side of Eq. (23) as:

$$\left(\prod_{j=0}^{K} d_j\right)^{\frac{1}{(K+1)}} \leq \frac{1}{(K+1)}\sum_{j=0}^{K} d_j; \tag{24}$$

consequently, if the following inequality

$$\frac{C_{ox}}{q}\sqrt{\frac{\sum_{j=0}^{K} jd_j}{2q\psi_B\varepsilon_{si}}}\times\left(\frac{kTm_{\max}}{q}\ln\left(\frac{\mu_{eff}C_{ox}\frac{W}{L}(m_{\max}-1)\left(\frac{kT}{q}\right)^2}{I_{off\text{-}set}}\right)-V_{fb}-2\psi_B\right)$$
$$\leq (K+1)\left(\prod_{j=0}^{K} d_j\right)^{\frac{1}{(K+1)}} \tag{25}$$

holds, then the inequality (23) is also achieved. The inequality (25) is a *posynomial* inequality, since the right-hand side is a *monomial* function and the left-hand side is a *posynomial* function with optimal variables d_j.

2.6. The formulated GP problem

From the *posynomial* function SS of Eq. (12), and the *posynomial* inequalities of I_{on} and I_{off} in Eqs. (19) and (25), respectively, the inverse doping profile problem (3) is now formulated as a GP problem:

$$\min\left\{2.3\frac{kT}{q}\left(1+\frac{3t_{ox}}{K}\sqrt{\frac{q\sum_{j=0}^{K} jd_j}{2\varepsilon_{si}\psi_B}}\right)\right\}$$

$$\text{s.t. } N_{\min}\leq d_j\leq N_{\max},\quad i=0,1,\ldots,K,$$

$$\frac{\sqrt{2q\psi_B\varepsilon_{si}}\sum_{j=0}^{K} d_j}{C_{ox}\left(V_{gs}-\sqrt{\frac{2m_{\max}I_{on\text{-}set}}{\left(\frac{W}{L}\right)\mu_{eff}C_{ox}}}-V_{fb}-2\psi_B\right)}\leq\sqrt{(K+1)\left(\prod_{j=0}^{K} jd_j\right)^{\frac{1}{(K+1)}}}$$

$$\frac{C_{ox}}{q}\sqrt{\frac{\sum_{j=0}^{K} jd_j}{2q\psi_B\varepsilon_{si}}}\left(\frac{kTm_{\max}}{q}\ln\left(\frac{\mu_{eff}C_{ox}\frac{W}{L}(m_{\max}-1)\left(\frac{kT}{q}\right)^2}{I_{off\text{-}set}}\right)-V_{fb}-2\psi_B\right)$$
$$\leq (K+1)\left(\prod_{j=0}^{K} d_j\right)^{\frac{1}{(K+1)}}, \tag{26}$$

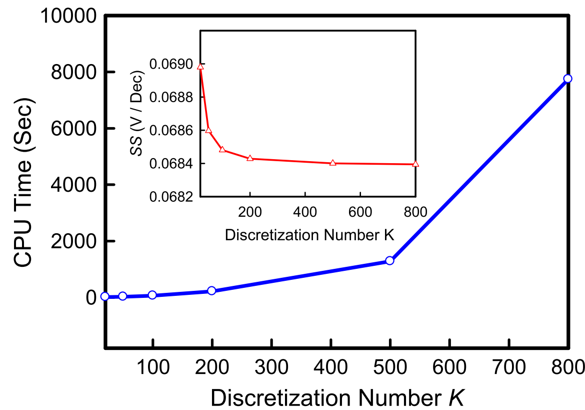

Fig. 3. The CPU time and the subthreshold swing (SS) as a function of discrete number K.

Table 1
The adopted physical parameters in the tested examples.

Symbol	Value
C_{ox}	4.13×10^{-7} F/C
t_{ox}	8 nm
V_{fb}	-0.97 V
ψ_b	0.4504 V
ε_{si}	1.04×10^{-12} F/cm^2
μ_{eff}	600 cm^2/V s
L	0.35 μm
W	1 μm
V_{dd}	3.3 V
$N_{\min}$	5×10^{16} cm^{-3}
$N_{\max}$	5×10^{19} cm^{-3}

which is a nonlinear constrained optimization problem and is also a GP problem with optimal variables: $d_j, j = 0, 1, \ldots, K$. The first expression is the objective function of subthreshold swing, the second and third inequalities are constraints of the on- and off-state state currents.

To solve the modeled GP problem, we mainly cast the GP problem (26) above into the convex programming problem [13]. Based upon duality theory of GP [13,23,24] and interior algorithm [13,25,26], the GP problem (26) could be solved efficiently and globally which is coded and solved together with the existing numerical solvers in GGPLAB [14]. The program is written by using Matlab® codes running on a personal computer. We discretize the problem with K varying from 20 to 800, and the corresponding CPU time and the objective value of SS are shown in Fig. 3. The CPU time grows exponentially when K increases which is directly proportional to the number of optimal variables d_j, but the objective value of SS is almost saturated when $K > 200$, as shown in inset of Fig. 3. As a result, for compromising computational cost and objective value, our following tested cases are all with $K = 200$. They have 200 variables and two nonlinear constraints and the computational time is of order of few minutes for different I–V specifications.

3. Results and discussion

In this section, we first discuss two numerical different examples: low-standby-power (LSP) and high-performance (HP) devices for the studied optimal doping profile problem (26), and then use numerical device simulation [20,21] to verify the accuracy of the GP optimized results including the sensitive analysis for the extracted optimal doping profiles. We consider examples for the optimal doping profile problem (26) for N-type MOSFET devices with 0.35-μm device channel length and 1-μm device width for different industrial purpose [1,2]. For LSP devices, high threshold voltage to suppress the standby-power consumption due to leakage current is necessary; without loss of generality, we set the specification of on- and off-state currents as: $(I_{off\text{-}set}, I_{on\text{-}set}) = (10^{-15}, 10^{-3}$ A) for LSP devices. For HP devices, it requires low threshold voltage to increase switching speed, and the specification of HP devices is assumed to be $(I_{off\text{-}set}, I_{on\text{-}set}) = (5 \times 10^{-11}, 2 \times 10^{-3}$ A) for HP devices. In these two tested examples, all adopted physical parameters from [1,2] are listed in Table 1.

The optimized doping profiles and corresponding I–V curves for the LSP (the solid lines) and HP (the dash lines) devices are shown in Fig. 4(a) and (b), respectively. The values of I–V characteristic are summarized in Table 2. For the LSP device, the threshold voltage is 1.1 V, and the off-state current is 2.5×10^{-16} A, which is smaller than the specified $I_{off\text{-}set} = 1 \times 10^{-15}$ A. For the HP device, it has small subthreshold swing and the threshold voltage is equal to 0.66 V, which has high operational

Table 2
Given targets and the GP optimized results of the LSP and HP devices.

	$I_{off\text{-}set}$ (A)	$I_{on\text{-}set}$ (A)	I_{off} (A)	I_{on} (A)
LSP	$\leq 1.1 \times 10^{-15}$	$\geq 1.0 \times 10^{-3}$	2.5×10^{-16}	2.4×10^{-3}
HP	$\leq 5.0 \times 10^{-11}$	$\geq 2.0 \times 10^{-3}$	3.1×10^{-12}	3.5×10^{-3}

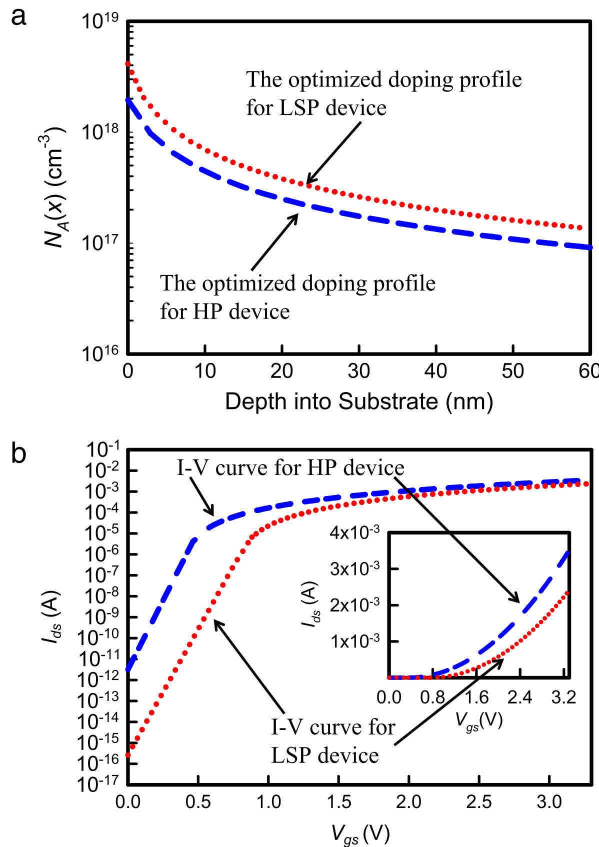

Fig. 4. (a) The optimized doping profiles of the tested LSP and HP N-type MOSFETs. (b) The corresponding I–V curves of the tested examples.

Table 3
The GP optimized result and the numerical device simulation.

	I_{on} (A)	I_{off} (A)	SS (V/Dec)	V_t (V)
$V_{ds} = 0.05$ (V)				
GP result	3.6×10^{-5}	6.5×10^{-16}	0.077	0.685
Device simulation	3.6×10^{-5}	6.2×10^{-16}	0.078	0.685
$V_{ds} = 3.3$ (V)				
GP result	6.1×10^{-4}	1.1×10^{-15}	0.077	0.669
Device simulation	6.0×10^{-4}	1.0×10^{-15}	0.075	0.671

speed as we expected owing to high on-state current, as shown in Fig. 4(b). The optimized HP device has a low concentration of doping profile, compared with the result of LSP, as shown in Fig. 4(a). The optimized high and low concentrations of doping profiles physically reflect the given specifications of low $I_{on\text{-}set}$ and high $I_{on\text{-}set}$ for LSP and HP devices, respectively.

We further verify the accuracy of the optimized 1D doping profile from the interface of silicon and silicon dioxide to substrate of the LSP device, the optimized doping profile is implemented and compared with the result from our own numerical semiconductor device simulator [20,21], where a set of classical DD equations is solved numerically. Fig. 5(a) shows the GP optimized and the calibrated doping profiles of the device simulation. The solid line shows the optimized doping profile and the dashed line shows the doping profile realized in the device simulations. In this device simulation, the mobility is with the value of 600 cm^2/V s as the same mobility setting in the GP model, as listed in Table 1 and the gate work

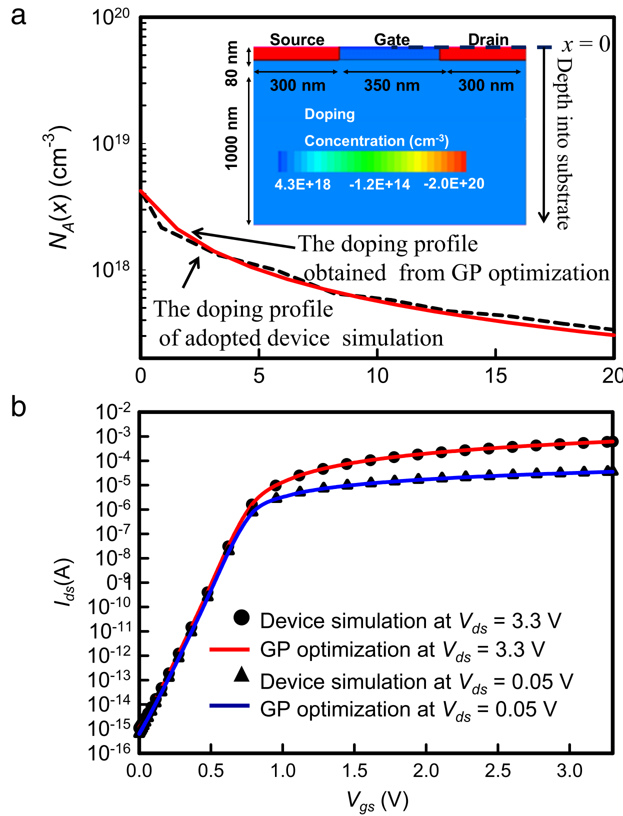

Fig. 5. (a) The doping distributions generated from the GP model and the device simulation, and the inset shows the simulated device structure of the explored MOSFET. (b) The I–V curves obtained by the GP model and the device simulation at different drain bias.

function is 4.1 eV. The I_{ds}-V_{gs} curves at two different drain biases (V_{ds}) are then extracted by the device simulation and the GP model, as shown in Fig. 5(b). The calibrated results are summarized in Table 3. The I–V characteristics of the GP optimization are in good agreement with the device simulation, for example, the different of threshold voltage at $V_{ds} = 3.3$ V between the GP model and device simulation is the almost the same, and when $V_{ds} = 0.05$ V, the threshold voltage from the GP model is 0.685 V which is similar to the threshold voltage 0.698 V simulated from the device simulation. The preliminary results confirm the accuracy of MOSFET's GP model.

For a purpose of engineering reference, we measure how sensitive the I–V characteristic is when variations occur in the doping concentration of source (S) and drain (D) at the same optimal doping profile in the channel:

$$\text{Sensitivity} = \left. \frac{\frac{\Delta(I\text{-}V\ characteristics)}{I\text{-}V\ characteristics}}{\frac{\Delta(S/D\ doping)}{S/D\ doping}} \right|_{N_A(x)} \times 100\%, \tag{27}$$

where the S/D doping denotes the doping concentration of source and drain, and we assume the variation of source/drain doping concentration is:

$$S/D\ \text{doping}^* = S/D\ \text{doping} \times 10^e, \tag{28}$$

where S/D doping* are the doping concentrations of source and drain after perturbation, e is a fractional error, and we assume $e \leq E$, where E is a maximum fractional deviation. For the worst case test, i.e., $e = E$, if we have a maximum deviation of 1, while fixing the extracted optimal channel doping profile, then we can calculate the sensitivity of the I–V characteristic under this perturbation of doping concentrations of source and drain. Fig. 6(a) shows the doping profiles of source and drain. The dashed lined is the nominal case of doping levels of source and drain which is equal to 5×10^{20} cm^{-3}, the dotted lined is the doping concentrations of source and drain after $e = 1$ increasing which is equal to 5×10^{21} cm^{-3}, and the solid lined shows the source/drain doping concentration after $e = -1$ reduction which is 5×10^{19} cm^{-3}. Fig. 6(b) shows the I–V curves under these three different doping concentrations of source and drain and the I–V characteristics are almost unchanged; for example, the sensitivity of the threshold voltage under this maximum perturbation of doping concentrations of source and drain is about ±0.005%. This shows that the I–V characteristic does not change appreciably with a variation in doping concentration of source and drain in our optimization.

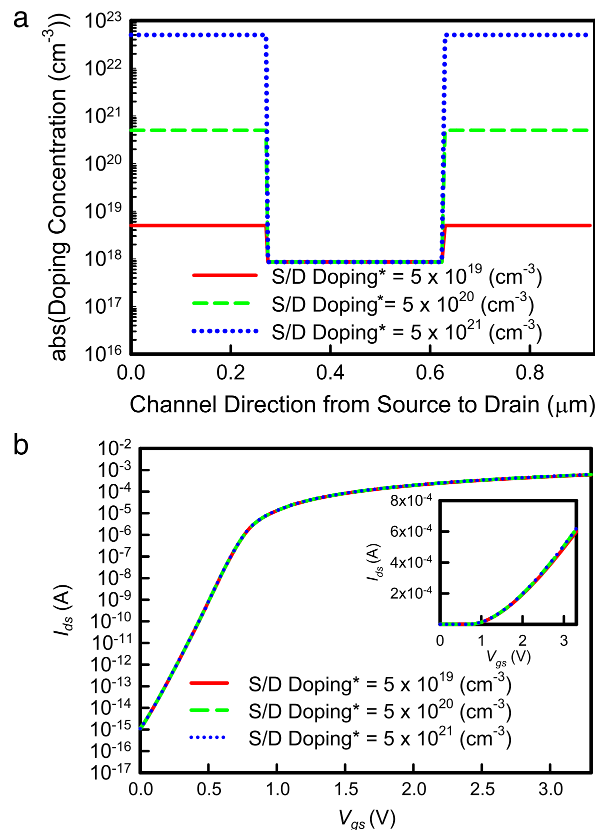

Fig. 6. (a) The source/drain doping profile ranging from 5×10^{19} to 5×10^{21} cm^{-3} for the sensitivity analysis of GP model. (b) The corresponding I–V curves in logarithm scale and linear scale.

4. Conclusions

We have shown the 1D channel doping profile optimization problem of N-type MOS device can be formulated according to desired targets into a GP problem. The GP problem is subject to constraints of background doping concentration and maximum doping level and on- and off-state currents while keeping subthreshold swing being minimized. The derived GP problem has been solved in a computationally effective manner which is proportional the number of discretized regions. The results of our tested examples show that it could be solved in seconds for appropriate discretization. This method can be used for P-type MOS devices. Short-channel effect plays an important role for deep-submicron MOSFET devices, so modeling 2D channel doping profile optimization into a GP problem is urgent. We are currently deriving MOSFET's GP problem for 2D structure considering random dopant induced threshold voltage fluctuation for nanometer-scale transistors.

Acknowledgment

The work was partially supported by the National Science Council (NSC), Taiwan, under Contract NSC-100-2221-E-009-018.

References

[1] S.M. Sze, Physics of Semiconductor Device, second ed., Wiley, New York, 1981.
[2] Y. Taur, T. Ning, Fundamentals of Modern VLSI Devices, Cambridge Univ. Press, Cambridge, UK, 1998.
[3] X.-H. Fu, J.-N. Chen, A point-by-point multiple-sweep numerical algorithm for dopant profiling based on C–V data, Solid State Electron. 35 (1992) 181–185.
[4] Z.K. Lee, M.B. McIlrath, D.A. Antoniadis, Inverse modeling of MOSFET's using I–V characteristics in the subthreshold region, in: IEEE International Electron Devices Meeting Tech. Digest, 1997, pp. 683–686.
[5] W. Kuzmicz, Application of a genetic algorithm to doping profile identification, J. Vac. Sci. Technol. B 14 (1) (1996) 408–413.
[6] Y. Li, S.M. Yu, A coupled-simulation-and-optimization approach to nanodevice fabrication with minimization of electrical characteristics fluctuation, IEEE Trans. Semicond. Manuf. 20 (4) (2007) 432–438.
[7] T. Binder, C. Heitzinger, S. Selberherr, A study on global and local optimization techniques for TCAD analysis tasks, IEEE Trans. Comput-Aided Des. Integr. Circuits Syst. 23 (6) (2004) 814–822.
[8] M. Burger, R. Pinnau, M.-T. Wolfram, On-/off-state design of semiconductor doping profiles, Commun. Math. Sci. 6 (2008) 1021–1041.

[9] A. Leitão, P.A. Markowich, J.P. Zubelli, On inverse doping profile problems for the stationary voltage-current map, Inverse Problems 22 (3) (2006) 1071–1088.
[10] P. Zhang, Y. Sun, H. Jiang, W. Yao, Multiscale methods for inverse modeling in 1-d MOS capacitor, J. Comput. Math. 21 (2003) 85–100.
[11] W. Fang, E. Cumberbatch, Inverse problems for metal oxide semiconductor field-effect transistor contact resistivity, SIAM J. Appl. Math. 52 (3) (1992) 699–709.
[12] S. Boyd, S.-J. Kim, L. Vandenberghe, A. Hassibi, A tutorial on geometric programming, Optim. Eng. 8 (1) (2007) 67–127.
[13] S. Boyd, L. Vandenberghe, Convex Optimization, Cambridge Univ. Press, Cambridge, UK, 2004.
[14] GGPLAB—a simple Matlab toolbox for geometric programming. [Online] http://www.stanford.edu/~boyd/ggplab/.
[15] Y. Li, Y.-C. Chen, C.-H. Hwang, Doping profile and Ge-Dose optimization for silicon–germanium heterojunction bipolar transistors, Semicond. Sci. Technol. 24 (10) (2009) 105020.
[16] S. Joshi, S. Boyd, R. Dutton, Optimal doping profiles via geometric programming, IEEE Trans. Electron Devices 52 (2005) 2660–2675.
[17] Y.-C. Chen, Y. Li, Temperature-aware floorplanning via geometric programming, Math. Comput. Modelling 51 (2010) 927–934.
[18] S. Boyd, S.-J. Kim, D. Patil, M. Horowitz, Digital circuits optimization via geometric programming, Oper. Res. 53 (6) (2005) 899–932.
[19] M. Hershenson, S. Boyd, T. Lee, Optimal design of a CMOS op-amp via geometric programming, IEEE Trans. Comput-Aided Des. Integr. Circuits Syst. 20 (1) (2001) 1–21.
[20] Y. Li, A parallel monotone iterative method for the numerical solution of multidimensional semiconductor poisson equation, Comput. Phys. Comm. 153 (2003) 359–372.
[21] Y. Li, S.M. Sze, T.S. Chao, A practical implementation of parallel dynamic load balancing for adaptive computing in VLSI device simulation, Eng. Comput. 18 (2002) 124–137.
[22] T.N. Nguyen, Small-Geometry MOS Transistors: Physics and Modeling of Surface- and Buried-Channel MOSFETs, Ph.D. Dissertation, Stanford Univ., Stanford, CA, 1984.
[23] M. Avriel, R. Dembo, U. Passy, Solution of generalized geometric programs, Int. J. Numer. Methods Eng. 9 (1996) 149–168.
[24] C.S. Beightler, D.T. Phillips, Applied Geometric Programming, Wiley, New York, 1976.
[25] K. Kortanek, X. Xu, Y. Ye, An infeasible interior-point algorithm for solving primal and dual geometric programs, Math. Program. 76 (1996) 155–181.
[26] O. Balm, J.L. Goffin, J.-Ph. Vial, O.Du. Merle, Experimental behavior of an interior point cutting plane algorithm for convex programming: an application to geometric programming, Discrete Appl. Math. 49 (1994) 2–13.